Journal of Hazardous Materials 332 (2017) 59–69

Contents lists available at ScienceDirect

Journal of Hazardous Materials

journal homepage: www.elsevier.com/locate/jhazmat

Photocatalytic degradation of 2-(4-methylphenoxy)ethanol over TiO_2 spheres

Marina Ilkaeva[a,b], Igor Krivtsov[a,b,*], Eva Díaz[c], Zakariae Amghouz[d], Yolanda Patiño[c], Sergei Khainakov[e], José R. García[a], Salvador Ordóñez[c]

[a] Department of Organic and Inorganic Chemistry, University of Oviedo-CINN, 33006, Oviedo, Spain
[b] Nanotechnology Education and Research Center, South Ural State University, 454080, Chelyabinsk, Russia
[c] Department of Chemical and Environmental Engineering, University of Oviedo, 33006, Oviedo, Spain
[d] Department of Materials Science and Metallurgical Engineering, University of Oviedo, Campus Universitario, 33203 Gijón, Spain
[e] Scientific Technical Services, University of Oviedo, 33006, Oviedo, Spain

HIGHLIGHTS

- The photocatalytic decomposition of an emerging pollutant 2-(4-methylphenoxy)ethanol (MPET) has been described.
- A toxic *p*-cresol is formed during the photodegradation of MPET.
- A method allowing converting nonporous titania spheres into a mesoporous material has been reported.
- The P25 and mesoporous TiO_2 spheres completely decompose MPET and *p*-cresol.
- Mesoporous TiO_2 spheres demonstrate superior to the P25 reusability.

GRAPHICAL ABSTRACT

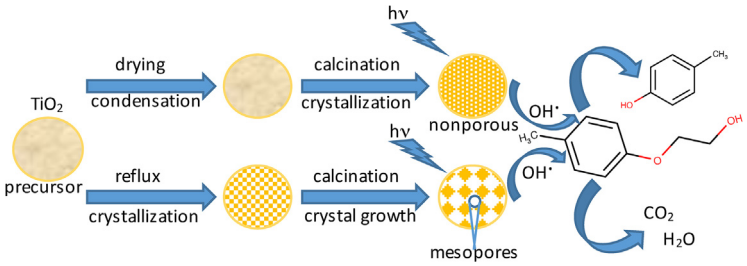

ARTICLE INFO

Article history:
Received 26 November 2016
Received in revised form 26 January 2017
Accepted 26 February 2017
Available online 1 March 2017

Keywords:
Emerging pollutants
Micropollutants
Titanium peroxo complex
Anatase-based photocatalysts

ABSTRACT

The photocatalytic TiO_2-assisted decomposition of 2-(4-methylphenoxy)ethanol (MPET) in aqueous solution has been studied for the first time. The intermediate compounds of MPET photodegradation have been also determined. A toxic *p*-cresol is formed in significant quantities during the photocatalytic reaction. A solvent-exchange approach for a template-free preparation of spherical TiO_2 particles has been described, which is based solely on precipitation of hydrous titania from aqueous titanium peroxo complex by using organic solvents. The proposed method favours the formation of spherical titania particles with a mean size varying from 50 to 260 nm depending on the choice of solvent. The procedure for converting nonporous titania spheres into mesoporous material maintaining the same spherical morphology has been developed. The synthesized TiO_2 spheres demonstrate a degree of MPET photo-degradation close to that of the commercial titania Aeroxide P25, besides being successfully recovered and reused for four reaction cycles without loss of photocatalytic activity. The effectiveness of the commercial Aeroxide P25 in MPET photodegradation, on the other hand, suffers 10-time drop during the third reaction cycle, which is attributed to its poor recoverability because the photocatalyst is composed of small particles of 20 nm size.

1. Introduction

Recent times have witnessed a fast development of industry promoted by invested capital, market growth and increased demands

* Corresponding author at: Department of Organic and Inorganic Chemistry, University of Oviedo-CINN, 33006, Oviedo, Spain.
E-mail addresses: uo247495@uniovi.es, zapasoul@gmail.com (I. Krivtsov).

http://dx.doi.org/10.1016/j.jhazmat.2017.02.055
0304-3894/

for new products. Thus, it is not surprising that a large and worrying number of emerging substances and pollutants is frequently encountered in waste waters, and so new measures must be taken for their removal. In particular, emerging pollutants, proceeding from cosmetic and chemical industries and usually found in water media, are undesirable compounds and considered harmful for the environment and human health. There are many ways suggested for their elimination, such as adsorption, advanced oxidation, photolysis, electrocatalysis, etc [1–5]. The main obstacle in the path of their removal is the low concentrations at which these emerging pollutants appear in aqueous solutions. One of these undesirable compounds is 2-(4-methylphenoxy)ethanol (MPET), and it is usually found in decorative cosmetics, fine fragrances, shampoos, toilet soaps, and other toiletries, as well as in non-cosmetic products, such as household cleaners and detergents. The worldwide consumption of MPET is close to 0.01–0.1 metric tons per year [6], so the interest in its removal from the environment is not surprising. Photocatalysis is known as an efficient oxidation process for degrading organic pollutants at low concentrations by transforming them into H_2O and CO_2. These transformations are conducted under conditions avoiding heating, high pressure, toxic chemicals or additives. Unfortunately, the decomposition process usually does not lead directly to the mineralization, but some oxidation by-products are also formed. Sometimes, intermediate compounds produced during the photooxidation processes can be even more hazardous than the initial pollutant, which makes their determination of key importance [7–9]. There is a considerable number of papers dealing with the selective photocatalytic oxidation of aromatic alcohols and ethers to the corresponding aldehydes [10–17]. However, to the best of our knowledge, this is the first study of photocatalytic decomposition of MPET focused on the total mineralization, revealing the formation of intermediates with their consecutive degradation pathway.

Titanium dioxide is the most widespread photocatalyst, which is due to its low-cost, non-toxicity and chemical stability, being attracted much attention recently [18–20]. Photocatalytic degradation of organic pollutants has become an extensive practice and special success has been achieved by Aeroxide P25 (Degussa P25) photocatalyst, which is due to the presence of anatase-rutile interface, its high crystallinity and relatively high surface area. However, the small particle size of Aeroxide P25 (around 20 nm) causes certain complications regarding the photocatalyst recovery and reuse. Unquestionably, the reusability of photocatalytic materials in the reaction cycles is required for the practical implementation of this technique. Several ways are proposed to achieve this aim, such as preparation of magnetic composite materials [21–25], thin film [26,27], and synthesis of sub-micron or micron-size spheres, which find their applications in many fields [28–35], but most importantly, spherical particles provide a desirable form for a solid catalyst facilitating its reuse [31,36,37]. The preparation of spherical titania particles demands special experimental setups or expensive (and occasionally volatile and toxic) organic structure-directing agents. The general procedures for the synthesis of TiO_2 spheres include the impregnation of hard template such as organic or silica spheres [38,39], soft template-assisted alkoxide-based sol-gel synthesis [40–42], or template-free approaches [43,44], using organometallic titanium sources, especially glycolate. While, only few preparation methods utilizing inorganic titania precursors are known [45], peroxo method is a good alternative to alkoxide-based or template-assisted procedures, since no toxic organic solvents or inert atmosphere are required. Titanium peroxo complexes are used for preparation of Na-titanates spherical particles [46] and TiO_2:Nb spheres *via* ultrasonic spray pyrolysis [47]. In the present study, we apply peroxo-mediated procedure for preparing TiO_2 spheres with controlled particle size and porosity, which is achieved by a choice of solvent used for the synthesis or by post-synthetic treatment.

2. Experimental

2.1. Materials

Titanium oxysulfate hydrate ($TiOSO_4 \cdot nH_2O$) and 30 wt% hydrogen peroxide were purchased from Aldrich. Hydrochloric acid 37–38 wt% water solution was obtained from J.T. Baker. Chloroform (99% purity), ammonium hydroxide 20 wt% water solution, methanol, ethanol and *n*-propanol (all VWR Chemicals) were of analytical grade and used as received without further purification. For the photocatalytic test, MPET of 98% purity was obtained from TCI Europe NV as well was 4-(2-hydroxyethoxy)-benzaldehyde (HEB). *p*-Cresol of 99% purity was purchased from Aldrich.

2.2. Synthesis

In this work we found that adjusting our previously reported method [48], by decreasing titania precursor concentration and increasing Ti:NH_3 ratio in the solvent-exchange preparation procedure, promoted formation of titania spherical particles.

Firstly, titanium hydroxide was precipitated from 25 mL of 0.1 M titanium oxysulfate solution by adding 2 mL of 20 wt% $NH_3 \cdot H_2O$ aqueous solution. The precipitate was centrifuged, washed and dissolved by adding 2.5 mL of 30 wt% hydrogen peroxide. The reaction mixture volume was adjusted to 25 mL by distilled water and pH value was set to 9.5 by adding ammonia. Then, the ice-cooled solution of peroxo complex was mixed with the equal volume of methanol, ethanol or *n*-propanol and then the suspension was formed. The obtained suspension was aged, isolated by centrifugation and washed with deionized water. The post-synthetic treatment of the titania spheres prepared in the presence of *n*-propanol was carried out in the following way: the amorphous precipitate, formed after *n*-propanol addition and aging for 24 h, was suspended in 50 mL of water-ethanol mixture (1:1 ratio by volume) at pH 4, which was adjusted by addition of HCl (1 M). The suspension was refluxed for 21 h and then the solid phase was separated by centrifugation at 3000 rpm and washed with deionized water. All precipitates were dried at 70 °C for 24 h before being subjected to investigation. Later, the samples were thermally treated in a muffle furnace at 500, 650 and 800 °C at a heating rate of 3 °C min^{-1} and calcination time of 30 min. The samples prepared by isolation of titania particles from the solutions containing methanol, ethanol, *n*-propanol and after the post-synthetic treatment were designated as TiMex, TiEtx, TiPrx, and TiPrRx, respectively, where "*x*" indicates the calcination temperature (in °C). The choice of the calcination temperature range was based on the previous study [48], where maximum photocatalytic activity was reached for the samples calcined at 800 °C.

2.3. Characterization

Powder XRD patterns were recorded in an X'pert PANanalytical diffractometer, using Ni-filtered Cu-Kα radiation source. The mean crystal sizes were calculated by Scherrer equation for anatase (101) reflection. A Shimadzu UV-2700 spectrophotometer with integrated sphere attachment was used to obtain diffusive reflectance spectra from the prepared oxides supported on the barium sulfate pellets. Band gap energy was estimated by applying Kubelka-Munk function to the DR UV spectra. SEM images were obtained by using a JEOL 6610LV scanning electron microscope; the samples were coated with gold prior to observation. Micromeritics ASAP 2020 was used to obtain adsorption-desorption isotherms of N_2 at 77 K.

Specific surface area (SSA) and pore size distribution were calculated from the low-temperature nitrogen adsorption data using BET and BJH approaches, respectively. Prior to the experiment the samples were outgassed under vacuum at 200 °C (for TiPrR) or 250 °C (for all other samples). TEM studies were performed on a JEOL JEM-2100F transmission electron microscope operated at accelerating voltage of 200 kV, equipped with a field emission gun (FEG) and with an ultra-high resolution pole-piece that provided point-resolution better than 0.19 nm. The samples for TEM were dispersed in ethanol, sonified and sprayed on a holey carbon film-coated copper grid and then allowed to air-dry; finally, Gatan SOLARUS 950 was used before observation. Point of zero charge (PZC) was measured using Zetasizer Nano ZS90.

2.4. Photocatalytic test

Photocatalytic properties of the prepared materials and the commercial Aeroxide P25 were investigated in the decomposition of MPET in aqueous-phase under UV-light. Since the as-prepared materials were amorphous, their photocatalytic tests were not performed. The UV-light source was a Helios Italquartz GR.E 500 W high-pressure mercury lamp (maximum radiation at 365 nm and impinging radiation was estimated to be 2.7 W m^{-2}) equipped with a Pyrex water-cooling jacket cutting-off the radiation wavelengths below 300 nm. In all experiments, 100 mg of sample was placed in a 250 mL Duran Glass reactor containing 200 mL of MPET solution in deionized water (20 mg L^{-1}). The reactor was set at 25 cm from the light source and the suspension was magnetically stirred. Firstly, adsorption of MPET on the titania samples was measured in the dark. After this, the suspension was exposed to UV-light and the aliquots of 3 mL were taken at appropriate intervals during the total irradiation time of 6 h if not stated otherwise. Then, the solution was filtered from the photocatalyst with 0.2 μm PTFE filter, extracted with chloroform (at volume ratio 1:1), and the concentrations of MPET and the reaction intermediate (*p*-cresol) were determined by GC–MS technique. A Shimadzu GC/MS QP2010 Plus system, equipped with 30 m long Teknokroma TRB-5MS capillary column, was previously calibrated by using standard solutions of the studied compounds. Photolysis of the MPET solution was carried out under the same experimental conditions, but in the absence of a photocatalyst. The total organic carbon (TOC) was measured using a Shimadzu TOC-V CSH Analyzer for the initial MPET solution, as well as after 360, 600, and 840 min of the photocatalytic reaction. Recyclability of the most active photocatalysts was tested in consecutive MPET photodecomposition cycles. For this purpose, the photocatalysts were separated from the reaction medium after 6 h of the reaction, by centrifugation at 3000 rpm for 3 min, then washed three times with deionized water, and dried at 70 °C for 48 h. The remaining amount of the photocatalyst was determined and reused in the following photodegradation runs.

The toxicity of the reaction solutions at different irradiation times was estimated according to the standard Microtox suggested protocol using a Microtox Model 500 Toxicity Analyzer [49]. The samples were placed in a 2% NaCl medium with an aliquot of marine bacterium *Vibrio fisheri* and the luminescence was measured after 5 and 15 min of incubation. The toxicity of water suspensions of Aeroxide P25 and TiPrR800 priory filtered through 0.2 μM PTFE filter was measured after 8 h of irradiation. Phenol and $ZnSO_4 \cdot 7H_2O$ were used as positive controls.

3. Results and discussion

3.1. Morphology and N_2 physisorption

The SEM images (Fig. 1) show that the particle size largely depends on the organic solvent used for the preparation. The samples prepared by adding methanol (TiMe) or ethanol (TiEt) to the peroxotitanium complex (PTC) solution have an average particle size of 50 nm (Fig. 1a, b), while this average is close to 200–300 nm (Fig. 1c) when *n*-propanol is used. The decrease in the overall particle diameter, as well as minor shape deformations are observed for the samples calcined at higher temperatures, as expected considering the sintetering and crystal growth (Fig. S1). It is worth mentioning that all prepared samples retain the spherical morphology up to 800 °C (Fig. S1). A similar effect of the solvent on the size of the spherical aggregates is observed for silica-titania spheres prepared *via* the peroxo method [50]. However, the formation of pure TiO_2 particles of the same shape in the absence of any silica source indicates that the assemblage of the spheres runs independently and it is not governed by Stöber process [51]. The particle size is an important property of any photocatalyst defining its reusability in consecutive reactions. For this reason, the TiPr sample has been chosen for the reflux treatment, due to its largest average spheres size. It should be mentioned that no significant difference has been observed between particle sizes of TiPr and TiPrR (Fig. 1c and d). According to SEM images, the spherical particles of TiMe, TiEt and TiPr possess smooth surface, whereas particles of TiPrR demonstrate remarkable roughness (Fig. 1). The samples calcined at 500 °C, which did not undergo the post-synthetic treatment, show comparatively low SSA values (16–35 $m^2 g^{-1}$) without suffering significant changes up to 800 °C (11–21 $m^2 g^{-1}$) (Table 1). Unsurprisingly, the lowest SSA has been found for the samples of TiPr series, which have the largest particle size (Table 1).

The effect of the post-synthetic treatment on the porosity of TiO_2 spheres is obvious, as SSA values reach 210 and 125 $m^2 g^{-1}$ for samples TiPrR and TiPrR500, respectively. Further increase of the calcination temperature up to 800 °C leads to crystal growth and pore shrinkage resulting in a substantial decrease of SSA down to 33 $m^2 g^{-1}$. The samples calcined without undergoing the post-synthetic treatment exhibit type-IV or type-III isotherm, according to IUPAC classification, with a barely distinguishable hysteresis loop in the range of P/P_0 0.90–0.99, which is an indication of the interparticle porosity (Figs. 2a and S2). The calcination temperature has a little influence on the porosity of TiPr samples, while the reflux treatment (TiPrR) reveals a drastic effect on it (Fig. 2). SSA of TiPr and TiPrR samples calcined at 500 °C (Table 1) differ by up to one order of magnitude. Moreover, the N_2 adsorption-desorption isotherm of the sample that underwent post-synthetic treatment features prominent hysteresis loop of H1-type at P/P_0 0.65–0.90, indicating the presence of the mesopores most likely to be attributed to the internal particle porosity. The pore size distribution analysis clearly demonstrates that TiPrR500 sample has a large mesopore volume (1.5 $cm^3 g^{-1}$) with a mean size of 10 nm, while this value is negligible for TiPr500 (Fig. 2a). Further heat treatment up to 800 °C for TiPrR800 has resulted in a significant reduction of SSA (Table 1) and pore volume (Fig. 2b); however, the SSA value of this sample is still higher than it is for the others treated under the same conditions. Also, despite the obvious deterioration of the textural properties, TiPrR800 retains the mesopores with an average size of 15 nm. From the N_2 physisorption analysis, it is clear that the proposed reflux treatment of the amorphous precursor results in enhancement of such desirable photocatalytic properties as mesoporosity and specific surface area.

3.2. XRD studies

In our previous work [48], we successfully synthesized nanoparticles of TiO_2 anatase stable up to 1000 °C by using a similar solvent-exchange method. In the present study, we have chosen lower calcination temperatures, because the TiO_2 nanoparticles treated at higher temperatures are less photocatalytically active [48]. Considering the previously obtained results, it is unsurprising

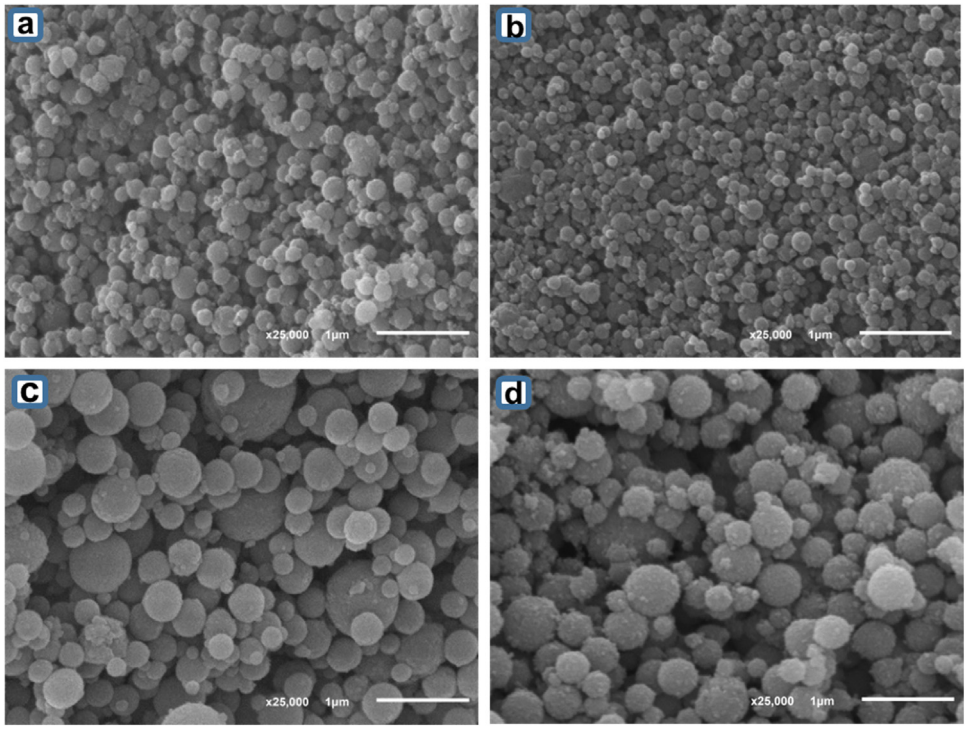

Fig. 1. SEM images of as-synthesized samples: TiMe (a), TiEt (b), TiPr (c), TiPrR (d).

Table 1
SSA, crystal size and band gap energy of the prepared photocatalysts.

sample	Treatment temperature (°C)									
	SSA (m^2 g^{-1})				Crystal size (nm)				Band gap (eV)	
	As prepared	500	650	800	As prepared	500	650	800	500	800
TiMe	–	29	31	21	–	26	28	44	3.28	3.23
TiEt	–	35	18	21	–	19	30	41	3.24	3.23
TiPr	–	16	13	11	–	23	25	41	3.31	3.24
TiPrR	210	125	84	33	6	11	15	37	3.40	3.24

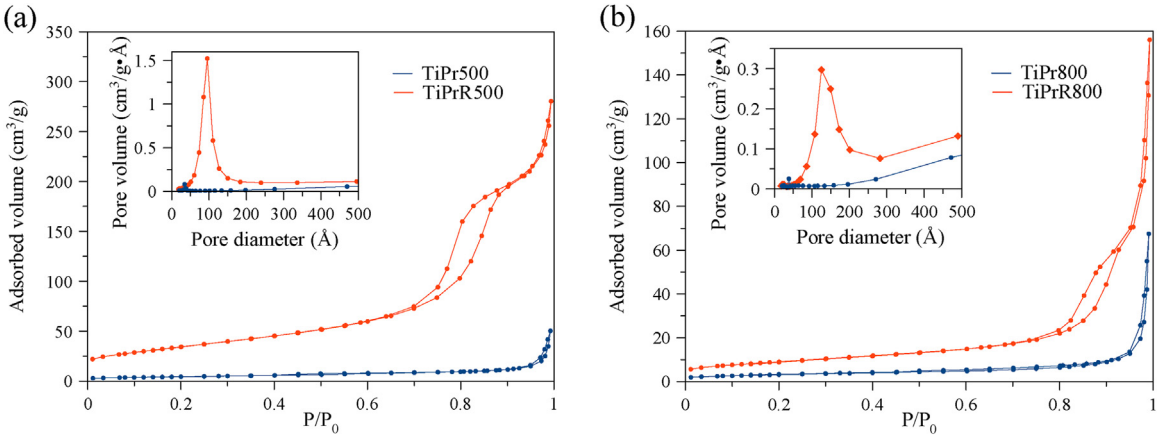

Fig. 2. N_2 adsorption-desorption isotherms and average pore size distribution of TiPrR and TiPr samples calcined at 500 °C (a) and 800 °C (b).

that all prepared samples show only the presence of anatase phase stable up to 800 °C (Fig. 3). The crystal sizes of TiMe, TiEt, and TiPr samples, calculated from the PXRD data by means of Scherrer equation, vary from 20 nm for the samples calcined at 500 °C up to 40 nm for those treated at 800 °C (Table 1). The sample that underwent the post-synthetic treatment (TiPrR) appears to have slightly different features. It is already crystalline after the reflux treatment and consequently its crystal growth under calcination follows a different mechanism, resulting in somewhat smaller crystal sizes (Table 1).

Normally the band gap energy of TiO_2 anatase is 3.2 eV, however, this parameter for the samples treated at 500 °C exceeds this value, and the presence of the defects in the crystal structure caused by the nitrogen incorporation, coming from ammonia used for the synthesis, is a possible reason for that [48]. Further heating to 800 °C

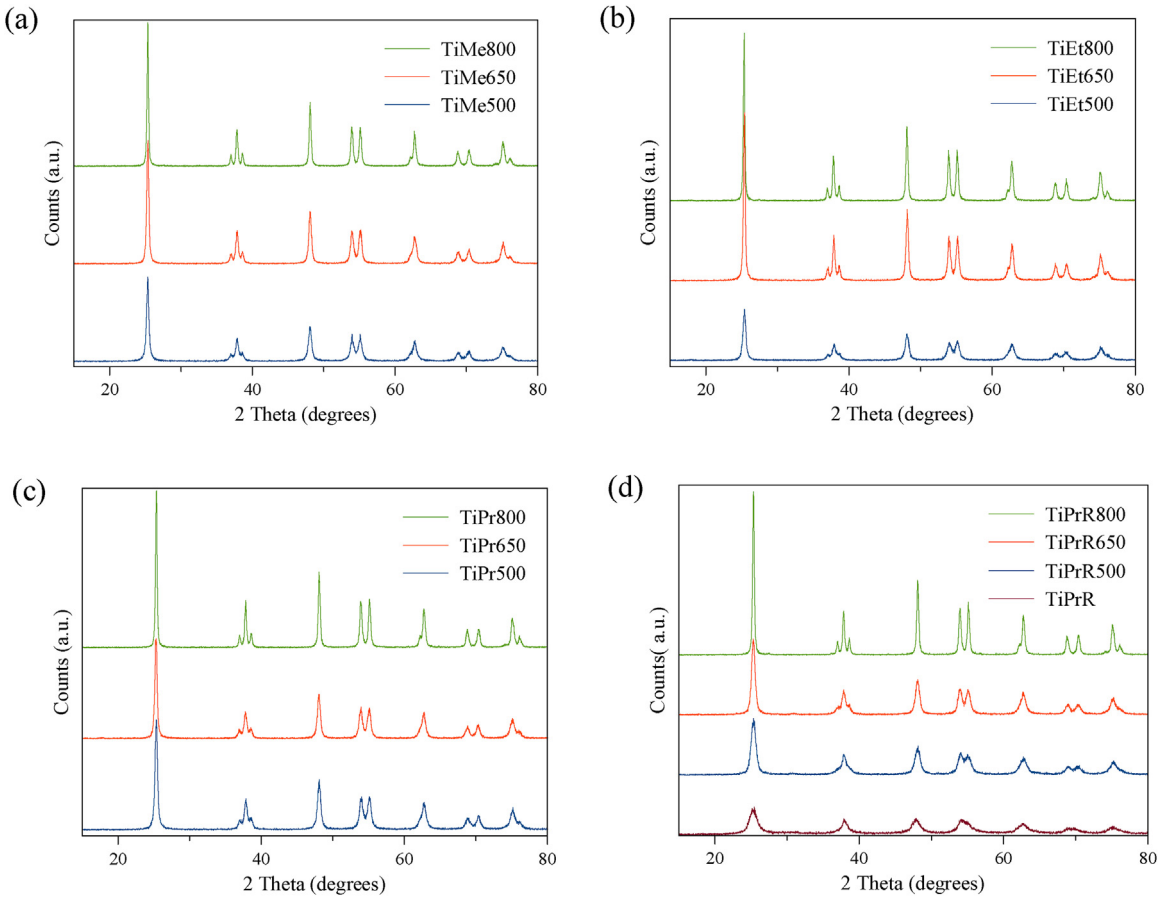

Fig. 3. PXRD patterns of TiMe (a), TiEt (b), TiPr (c), and TiPrR (d) samples at different calcination temperatures.

promotes the narrowing of the band gap value by eliminating the crystal defects (Table 1).

3.3. TEM studies

As it has been discussed in subsections 3.1 and 3.2, the spherical particles prepared by the proposed technique demonstrate very similar structural and morphological features, which are only modified by the post-synthetic treatment. In the same way, similar materials in a nanoparticulate form have the highest photocatalytic activity when they are calcined at 800 °C [48]. Therefore, TiPr, TiPr800, TiPrR and TiPrR800 samples were selected to be studied in more detail using TEM. For instances, Fig. S3 represents the particle-size histograms of samples TiPr (a), TiPr800 (b), TiPrR (c), and TiPrR800 (d) determined by counting more than 180 particles. The solid blue line corresponds to the Log-normal distribution function fit with a mean size of 0.17(1), 0.21(3), 0.263(7) and 0.262(3) μm, respectively (Table S1). As it was expected, the spherical particles of TiPr sample are totally amorphous according to selected area electron diffraction (SAED) patterns and HRTEM images (Fig. 4a). While in the case of TiPr800 sample, we can clearly observe aggregates made up of densely packed TiO_2 nanocrystals, forming spherical particles (Fig. 4b). Both particle and crystal sizes are in good agreement with SEM and XRD data, respectively. SAED pattern (Fig. 4b) shows the polycrystalline nature of the spherical particles and all the observed diffraction rings have been unambiguously assigned to the anatase phase (a = 3.776 Å, b = 9.486 Å, space group $I4_1/amd$; ICSD PDF4: 002-0406) in agreement with its simulated pattern, being Miller indices depicted. Similarly, HRTEM images (for instances Fig. 4b) prove the highly crystalline nature of these TiO_2 nanoparticles with an interplanar spacing of 3.51 Å characterizing the anatase TiO_2 {101} facet. Furthermore, the spheres formed after the post-synthetic treatment (TiPrR) are already crystalline as confirmed by SAED pattern (Fig. 5a). The HRTEM images (Fig. 5a) show the presence of small TiO_2 nanocrystals of approximately 10 nm, which are loosely assembled in these spherical aggregates, whereas thermal treatment at 800 °C (TiPrR800) provokes the growth of the nanocrystallites up to 50 nm, but maintaining the average size of the spheres (see Fig. S3), and hence reducing the internal porosity of the spherical particles (Fig. 5b); however, more loose assembly of TiO_2 nanocrystals is still obviously manifested compared to that of TiPr800.

Summarizing the data obtained using the characterization methods described in subsections 3.1–3.3, one can conclude that the prepared samples are composed solely of the anatase phase and they have insignificant differences in many structural features, such as unit cell parameters (Table S2) or band gap values (Table 1). Though the titania samples might be structurally identical, the dissimilarity of their particle sizes, SSA and pore sizes can affect the photocatalytic properties to a large extent.

3.4. Photocatalytic degradation of MPET

Before starting to study the photocatalytic properties of the prepared titania materials, the photolysis of MPET in aqueous solution and its adsorption were measured. The photolysis was found to be responsible for the decrease of only 2.5% of MPET initial concentration, while its adsorption on all investigated samples did not exceed 1%.

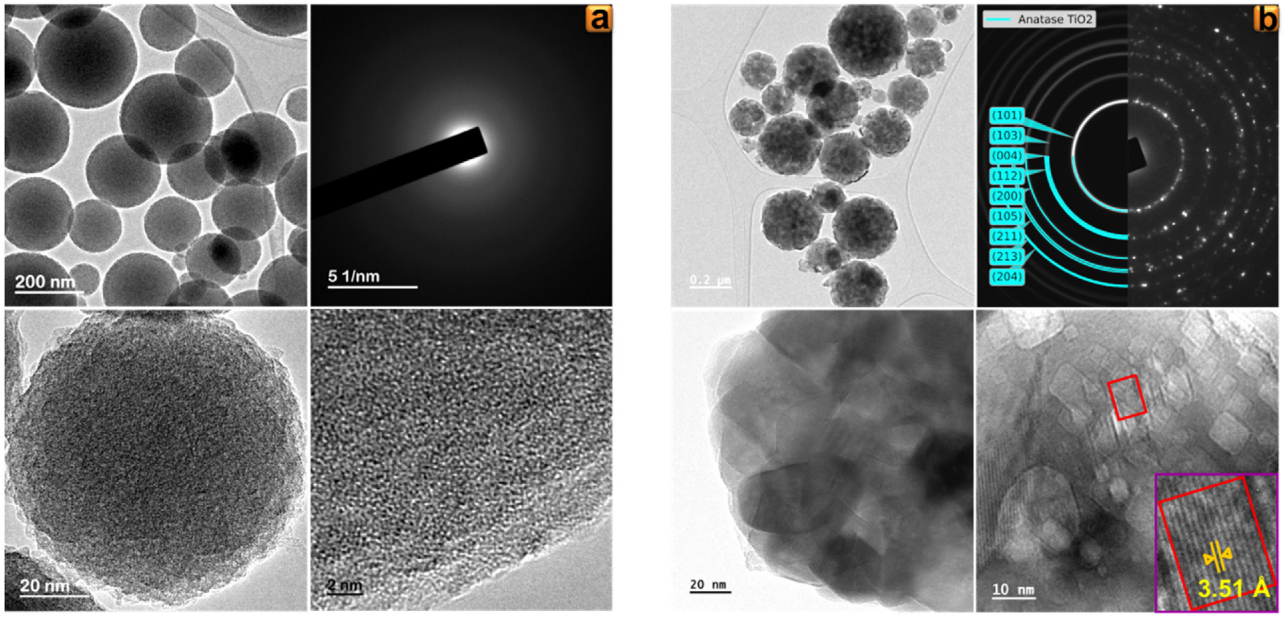

Fig. 4. TEM images and SAED patterns (experimental and simulated) of TiPr (a) and TiPr800 (b) samples.

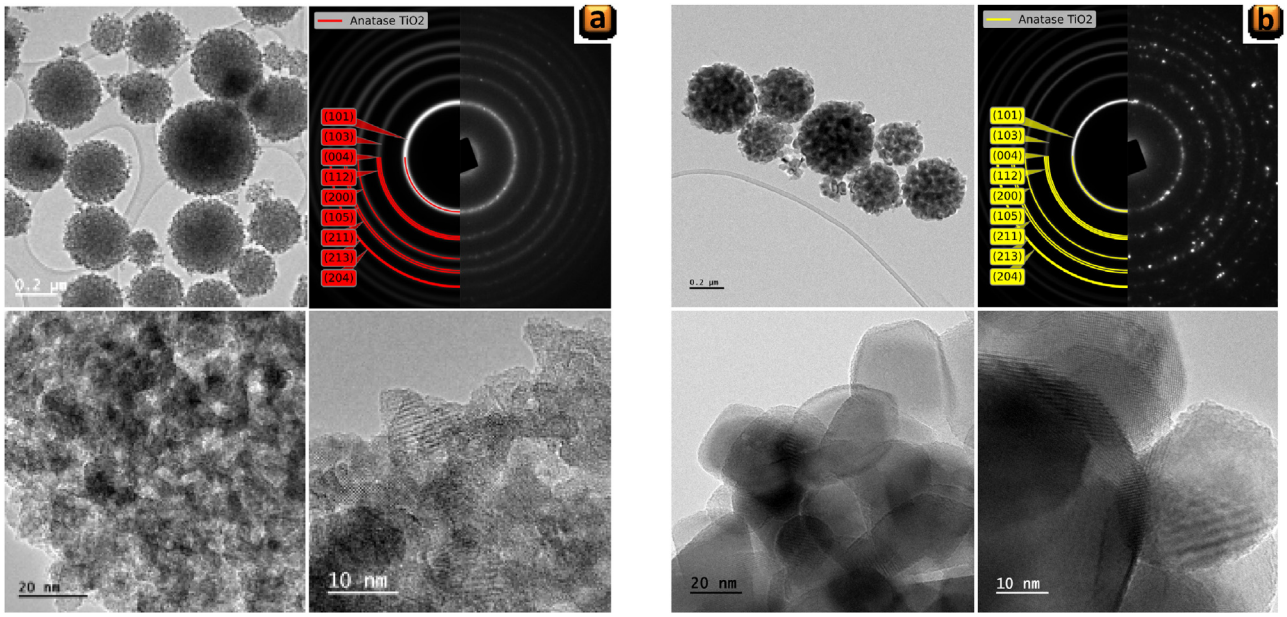

Fig. 5. TEM images and SAED patterns (experimental and simulated) of TiPrR (a) and TiPrR800 (b) samples.

Table 2
First-order kinetic constant k1 (min^{-1}) of MPET degradation and correlation coefficient R.

	TiMe		TiEt		TiPr		TiPrR		Aeroxide P25	
	k1	R	k1	R	k1	R	k1	R	k1	R
As-prepared	–	–	–	–	–	–	0.0046	–	0.0263	0.96
500 °C	0.0015	0.94	0.0012	0.98	0.0011	0.99	0.0074	0.94	–	–
650 °C	0.0040	0.98	0.0038	0.99	0.0034	0.99	0.0093	0.99	–	–
800 °C	0.0053	0.99	0.0059	0.99	0.0060	0.99	0.0139	0.96	–	–

The TiO_2 spheres, calcined at the same temperatures and which have not undergone the post-synthetic treatment, show similar performance in the UV-assisted degradation of MPET (Fig. 6, Table 2). The highest values of MPET removal (ca. 80%) are reached for this type of the samples thermally treated at 800 °C, and the same effect of calcination temperature was observed earlier for TiO_2 nanoparticles [48].

Also, MPET degradation rate shows its dependence on the calcination temperature for the refluxed TiO_2 anatase spheres (Fig. 6). The photocatalytic activity of this sample rises along with the increase of titania crystal size, despite the loss of SSA (Fig. S4).

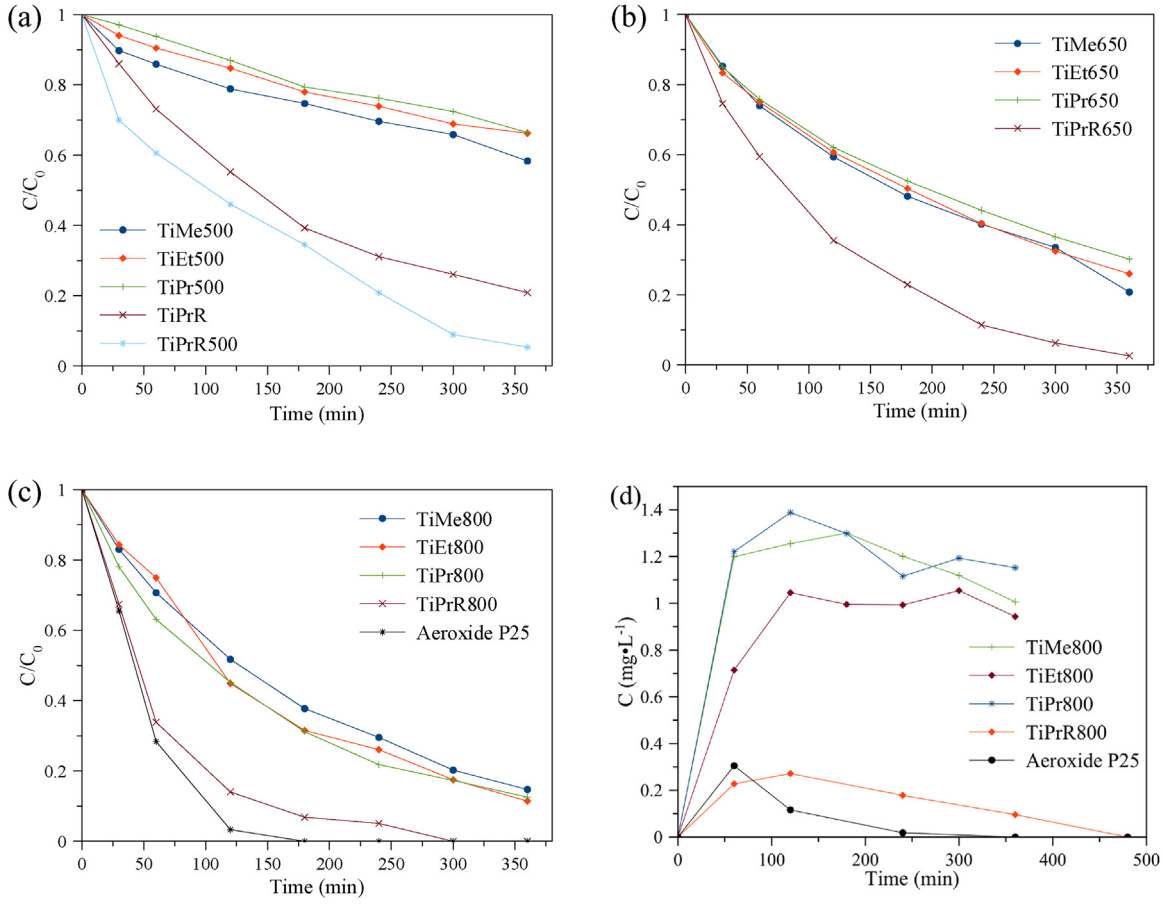

Fig. 6. Degradation curves of MPET under UV-light in the presence of the samples: calcined at 500 °C (a), 650 °C (b), 800 °C (c), Aeroxide P25 (c), and *p*-cresol evolution curves in the presence of different photocatalysts (d).

In the previous work, we found that small amounts of nitrogen is retained in the samples prepared by the precipitation from titanium peroxo complex and calcined at temperatures not higher than 500 °C [48]. This fact indicates that the crystal defects, are probable centres of electron-hole pairs recombination, caused by nitrogen-doping or the crystal growth process, are gradually eliminated at elevated temperatures. Obviously, the performance of TiPrR samples in MPET photodegradation is better than the titania spheres, which have not undergone the post-synthetic treatment, and the total decomposition of the substrate is achieved after 300 min of UV irradiation for TiPrR800, considered the most active sample of this series (Fig. 6c). By considering that the major difference between the samples, directly calcined after the synthesis and previously refluxed, is due to their SSA and pore size distribution, so it is logical to suggest that the enhanced photodegradation rate observed for TiPrR samples is derived from the accessibility of the photocatalyst's surface to MPET molecules. We suggest that the decisive role in the improved reaction performance is played by the pores with diameters between 10 and 20 nm, formed as a consequence of the post-synthetic treatment (Fig. 2). The commercial TiO_2 Aeroxide P25 is considered as the "gold standard" because of its outstanding photocatalytic activity under UV irradiation, which is due to the presence of anatase-rutile interface and its high crystallinity and good dispersibility in a liquid media. In the studied reaction, Aeroxide P25 proves itself as a highly efficient material capable of complete decomposition of MPET in 180 min under UV irradiation (Fig. 6c, Table 2).

In order to thoroughly evaluate the photocatalytic activity of such compounds, it is not enough to track the decomposition of a substrate, but it is also very important to determine the reaction pathways and intermediate compounds formed during the photodegradation process. We have detected four major intermediate aromatic compounds during MPET photodecomposition, which include *p*-cresol **(2)**, *p*-methylphenoxyacetaldehyde **(3),** *p*-methylcatechol **(4)** and HEB (**5**) (Scheme 1). The degradation pathways are depicted in Scheme 1 and the mass spectra of the compounds are presented in the SI (Fig. S5). Unsurprisingly, the elimination of ether group is the prevailing decomposition pathway, the same observations were made by Bahnemann et *al.* when studied phenoxyacetic acid photodegradation [52]. The rupture of the ether bond favours the formation of *p*-cresol (**2**), which is the dominant intermediate of this reaction. *p*-Cresol is a toxic compound which presence in water is highly undesirable. According to United States Environmental Protection Agency (USEPA), aquatic organisms should not be affected unacceptably if the four-day average concentration of *p*-cresol does not exceed 53 μg/L more than once every three years on the average and if the one-hour average concentration does not exceed 480 μg/L more than once every three years on the average [53]. This indicates on a serious problem of eliminating not only the initial emerging pollutant, but the toxic intermediate at a very low concentration level as well [54–57]. Most of the tested photocatalysts do not guarantee the complete elimination of *p*-cresol (**2**) during the reaction time (Fig. 6d). Aeroxide P25 is capable of totally decomposing MPET, as well as *p*-cresol (**2**), within 360 min, while TiPrR800 reaches this level of performance after 480 min of UV irradiation (Figs. 6d). The *p*-cresol (**2**) decomposition also has its sub-product, as the benzene ring hydroxylation takes place, thus *p*-methylcatechol (**4**) is

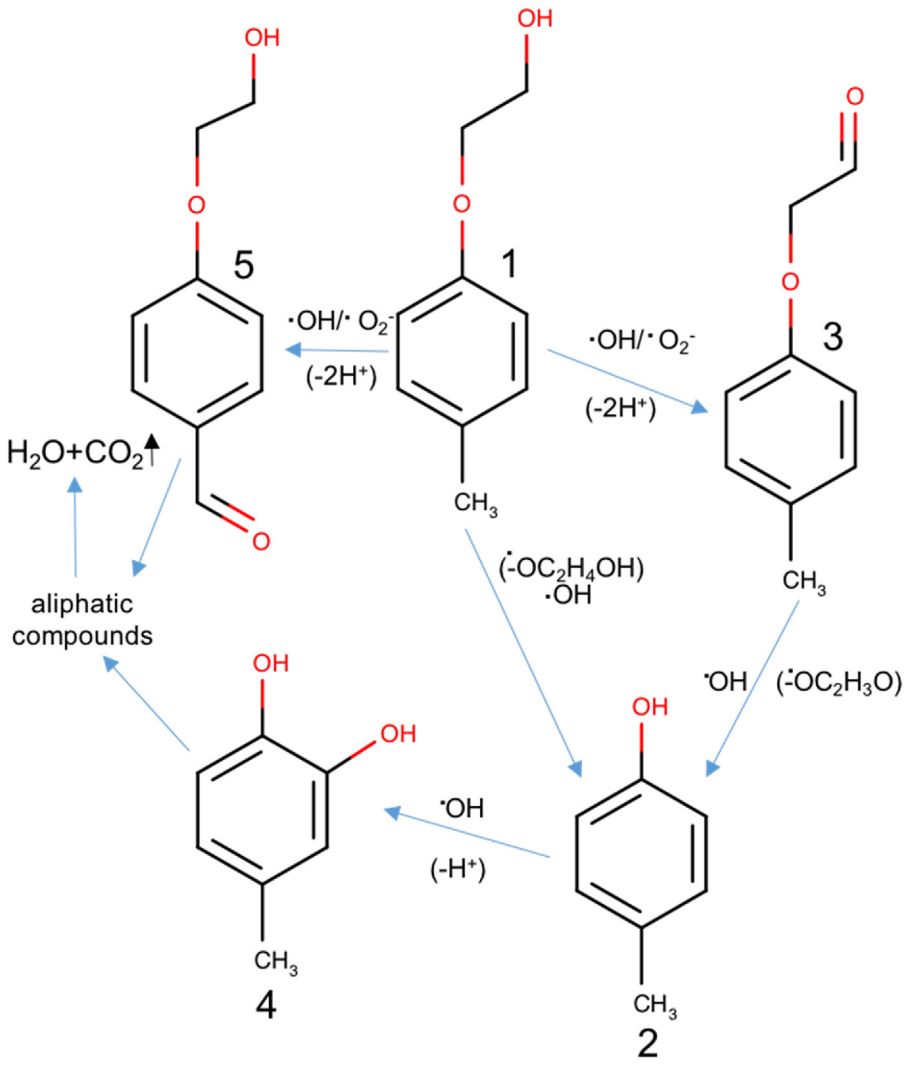

Scheme 1. MPET photocatalytic degradation pathway.

formed. However, *p*-methylcatechol (**4**) is produced in trace quantities, and it is decomposed somewhat faster than *p*-cresol (**2**), due to the lower stability of the more hydroxylated benzene ring.

The formation of *p*-methylphenoxyacetaldehyde (**3**) and HEB (**5**) is less favourable than that of *p*-cresol (**2**), due to the presence of weak ether group, which is susceptible to interact with reactive species. The oxidation of MPET to the compound (**3**) evolves according to the mechanism described by Bahnemann et al. [16,17], while (**5**) is produced by oxidation of methyl group of MPET. Then compound (**3**) is decomposed to *p*-cresol (**2**) through the ether bond breaking mechanism, while (**5**) by oxidizing is most likely to produce aliphatic compounds, since no 4-hydroxybenzaldehyde is detected (Scheme 1). Also, we have found that the degradation of MPET is accompanied by a slight reduction of pH of the suspension from 5.5 to 4.1, which is superior or equal to the PZC of TiPrR800 having a value of 4.1 (Fig. S6). The mineralization of MPET into CO_2 and H_2O was estimated by TOC measurement. The TOC removal data follow the same pattern as the MPET degradation curves. The highest value of the substrate mineralization is observed for P25 photocatalyst (63% after 6 h), followed by TiPrR800 with 36% (Fig. 7a). TiPrR800 sample appears to be the most active photocatalyst among all synthesized samples (Fig. 7a). Extending the irradiation time up to 14 h in the presence of TiPrR800 allows achieving the TOC removal of 57%, which is close to the value obtained for P25 within 6 h (Fig. 7b). Although the P25 might seem an ideal photocatalyst, it has a very notable drawback complicating its implementation in real-life applications. Due to its small particle size of about 20 nm and, consequently, high dispersibility in the liquid media, it suffers from poor recyclability or demands special measures for its separation after the photocatalytic reaction [58]. As it is shown in Figs. 8 and S7, more than a half of the starting amount of P25 used is lost after the first reaction cycle; however, P25 retaines a high level of activity. Then, almost all the P25 catalyst is washed away after the second reaction run, leading to the drastic loss of activity.

On the other hand, the titania spheres maintain their morphology after the reaction runs (Fig. S8) and demonstrate more stable performance during four consecutive cycles, retaining 60% of the starting amount of the photocatalyst after the fourth reaction run and maintaining TOC removal between 32 and 41% (Figs. 8 and S7).

Evidently, the photooxidation of MPET is a complex process leading to the formation of a variety of aromatic and aliphatic intermediates, making it difficult to establish a level of harm each compound might cause in the environment. Hence, the estimation of toxicity is necessary to ensure viability of the proposed materials and photodegradation method. Fig. 9 demonstrates that P25 Aeroxide gradually reduces toxicity of the initial MPET solution, while TiPrR800 produces more toxic partial oxidation compounds after 2 and 4 h of the reaction, but finally degrading them, thus lowering the toxicity below the starting value. Higher toxicity of

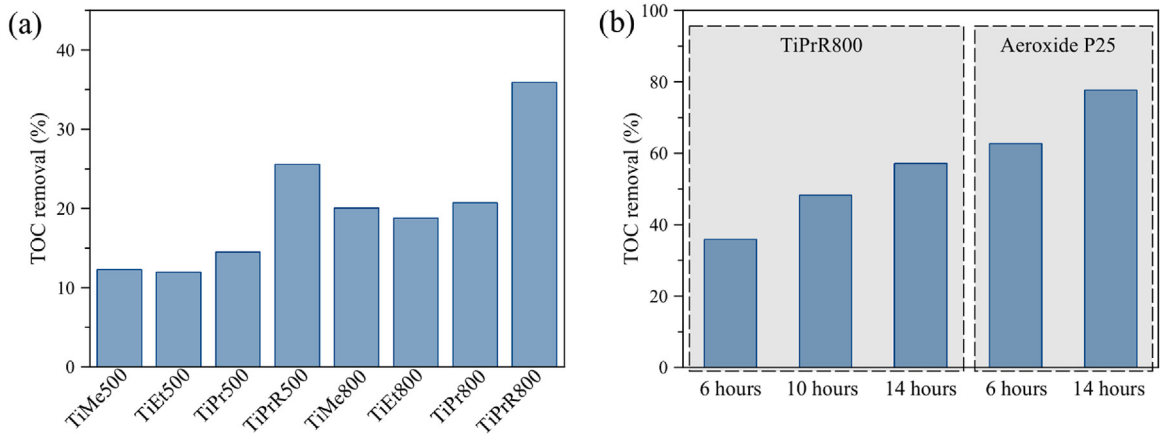

Fig. 7. TOC removal data for the synthesized samples after 6 h of the reaction (a) and at different reaction time (b).

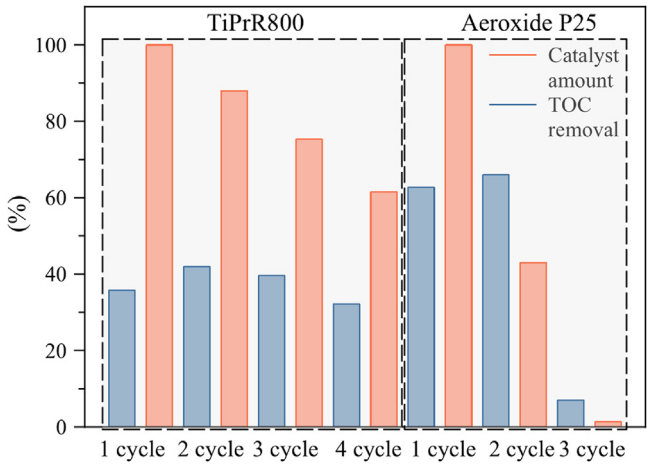

Fig. 8. TOC removal and amounts of TiPrR800 and Aeroxide P25 photocatalysts during 4 consecutive reaction cycles.

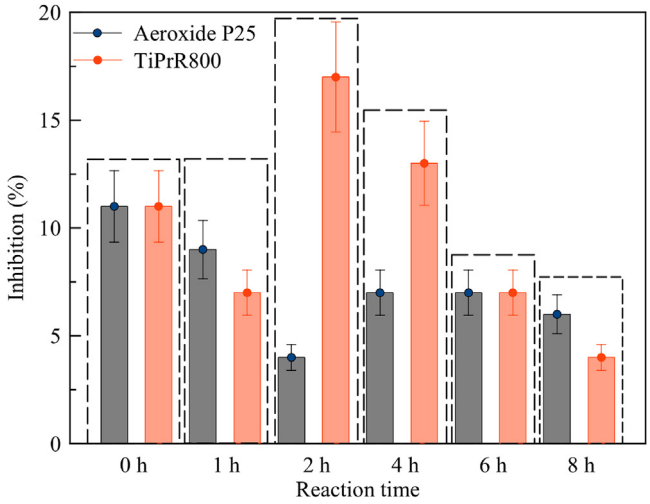

Fig. 9. % Inhibition of bioluminescence of *Vibrio fischeri* bacteria as a function of photocatalytic treatment in the presence of Aeroxide P25 and TiPrR800.

the partial oxidation products of TiO_2-assisted photo-degradation of herbicides and pharmaceuticals than the substrates themselves was attributed by Antonopoulou et al. to the synergetic effect of several reaction intermediates [59,60]. The similar effect might take place in the present case, as the maximum of toxicity for the solutions photocatalytically treated in the presence of TiPrR800 is found for the 2 h of irradiation, which coincides with the reaction time when the highest concentration of the major oxidation side-product is observed (Fig. 6d), however we cannot attribute this increased toxicity to any certain compound (Fig. S9). Besides the toxicity of the organic compounds formed during the reaction, the possible influence of photocatalyst particles on the inhibition of the bacteria is also must be estimated. The disaggregation of the photocatalysts takes place under the UV-irradiation, and some small nanoparticles might be able to pass the filtering systems. The toxicity of filtered water suspensions of the commercial photocatalyst and titania spheres after the UV-irradiation shows higher inhibition of the bacteria in case of Aeroxide P25 (Fig. S10). This finding is in accordance with other works demonstrating significant toxic effect of TiO_2 nanoparticles on live organisms [61,62].

4. Conclusions

We have demonstrated that the use of aliphatic alcohols with different carbon chain length, during the solvent-exchange procedure, allows manipulating the particle size of the TiO_2 spheres. The resulted titania photocatalysts are mildly active due to their nonporous nature. However, the developed post-synthetic reflux procedure successively converts the prepared titania spheres into more efficient photocatalytic mesoporous material.

The determined pathway of MPET photocatalytic decomposition, under UV-light and assisted by TiO_2 photocatalysts, includes the formation of toxic *p*-cresol intermediate. It has been established that the commercial photocatalyst Aeroxide P25 and the prepared mesoporous TiO_2 spheres are able to decompose totally and efficiently the initial substrate as well as the intermediate *p*-cresol, thus leaving no toxic compounds behind after the photocatalytic reaction. Although the above-mentioned photocatalysts are both effective, the synthesized mesoporous titania spheres have an advantage over P25, since they are easily separated from the reaction mixture after the photocatalytic run, hence they can be reused multiple times without losing their activity.

Acknowledgements

We gratefully acknowledge financial support from the Spanish MINECO (MAT2016-78155-C2-1-R, MAT2013-40950-R, CTQ2011-29272-C04-02), and the Government of the Principality of Asturias (GRUPIN14-060; GRUPIN14-078; and "Severo Ochoa" PhD grantBP-14-029 to M.I.) and FEDER. South Ural State University acknowledges financial support from Ministry of Education and Science of the Russian Federation (grant No 16.2674.2014/K). IK is

grateful for the support by Act 211 Government of the Russian Federation, contract № 02.A03.21.0011. We thank Cogersa for carrying out the toxicity measurements.

Appendix A. Supplementary data

Supplementary data associated with this article can be found, in the online version, at http://dx.doi.org/10.1016/j.jhazmat.2017.02.055.

References

[1] Y. Patiño, E. Díaz, S. Ordóñez, Performance of different carbonaceous materials for emerging pollutants adsorption, Chemosphere 119 (2015) 124–130.
[2] Y. Patiño, E. Díaz, S. Ordóñez, E. Gallegos-Suarez, A. Guerrero-Ruiz, I. Rodríguez-Ramos, Adsorption of emerging pollutants on functionalized multiwall carbon nanotubes, Chemosphere 136 (2015) 174–180.
[3] S. Esplugas, D.M. Bila, L.G.T. Krause, M. Dezotti, Ozonation and advanced oxidation technologies to remove endocrine disrupting chemicals (EDCs) and pharmaceuticals and personal care products (PPCPs) in water effluents, J. Hazard. Mater. 149 (2007) 631–642.
[4] H.-S. Chang, K.-H. Choo, B. Lee, S.-J. Choi, The methods of identification analysis, and removal of endocrine disrupting compounds (EDCs) in water, J. Hazard. Mater. 172 (2009) 1–12.
[5] Q. Wang, T. Jin, Z. Hu, L. Zhou, M. Zhou, TiO_2-NTs/SnO_2-Sb anode for efficient electrocatalytic degradation of organic pollutants: effect of TiO_2-NTs architecture, Sep. Purif. Technol. 102 (2013) 180–186.
[6] R.I.F.M. Expert Panel, D. Belsito, D. Bickers, M. Bruze, P. Calow, M.L. Dagli, A.D. Fryer, H. Greim, Y. Miyachi, J.H. Saurat, I.G. Sipes, A toxicological and dermatological assessment of aryl alkyl alcohols when used as fragrance ingredients, Food Chem. Toxicol. 50 (2012) S52–S99.
[7] A.O. Kondrakov, A.N. Ignatev, F.H. Frimmel, S. Bräse, H. Horn, A.I. Revelsky, Formation of genotoxic quinones during bisphenol A degradation by TiO_2 photocatalysis and UV photolysis: a comparative study, Appl. Catal. B: Environ. 160–161 (2014) 106–114.
[8] G. Li, X. Nie, Y. Gao, T. An, Can environmental pharmaceuticals be photocatalytically degraded and completely mineralized in water using g-C_3N_4/TiO_2 under visible light irradiation?—Implications of persistent toxic intermediates, Appl. Catal. B: Environ. 180 (2016) 726–732.
[9] W.M.M. Mahmoud, A.P. Toolaram, J. Menz, C. Leder, M. Schneider, K. Kummerer, Identification of phototransformation products of thalidomide and mixture toxicity assessment: an experimental and quantitative structural activity relationships (QSAR) approach, Water Res. 49 (2014) 11–22.
[10] S. Yurdakal, G. Palmisano, V. Loddo, V. Augugliaro, L. Palmisano, Nanostructured rutile TiO_2 for selective photocatalytic oxidation of aromatic alcohols to aldehydes in water, J. Am. Chem. Soc. 130 (2008) 1568–1569.
[11] I. Tamiolakis, I.N. Lykakis, G.S. Armatas, Mesoporous CdS-sensitized TiO_2 nanoparticle assemblies with enhanced photocatalytic properties: selective aerobic oxidation of benzyl alcohols, Catal. Today 250 (2015) 180–186.
[12] G. Palmisano, S. Yurdakal, V. Augugliaro, V. Loddo, L. Palmisano, Photocatalytic selective oxidation of 4-methoxybenzyl alcohol to aldehyde in aqueous suspension of home-prepared titanium dioxide catalyst, Adv. Synth. Catal. 349 (2007) 964–970.
[13] V. Augugliaro, H. Kisch, V. Loddo, M.J. López-Muñoz, C. Márquez-Álvarez, G. Palmisano, L. Palmisano, F. Parrino, S. Yurdakal, Photocatalytic oxidation of aromatic alcohols to aldehydes in aqueous suspension of home-prepared titanium dioxide: 1. Selectivity enhancement by aliphatic alcohols, Appl. Catal. A 349 (2008) 182–188.
[14] M. Addamo, V. Augugliaro, M. Bellardita, A.D. Paola, V. Loddo, G. Palmisano, L. Palmisano, S. Yurdakal, Environmentally friendly photocatalytic oxidation of aromatic alcohol to aldehyde in aqueous suspension of brookite TiO_2, Catal. Lett. 126 (2008) 58–62.
[15] I. Tamiolakis, I.N. Lykakis, A.P. Katsoulidis, G.S. Armatas, One-pot synthesis of highly crystalline mesoporous TiO_2 nanoparticle assemblies with enhanced photocatalytic activity, Chem. Commun. 48 (2012) 6687–6689.
[16] M. Qamar, R.B. Elsayed, K.R. Alhooshani, M.I. Ahmed, D.W. Bahnemann, Chemoselective and highly efficient conversion of aromatic alcohols into aldehydes photo-catalyzed by Ag_3PO_4 in aqueous suspension under simulated sunlight, Catal. Commun. 58 (2015) 34–39.
[17] M. Qamar, R.B. Elsayed, K.R. Alhooshani, M.I. Ahmed, D.W. Bahnemann, Highly efficient and selective oxidation of aromatic alcohols photocatalyzed by nanoporous hierarchical Pt/Bi_2WO_6 in organic solvent-free environment, ACS Appl. Mater. Interfaces 7 (2015) 1257–1269.
[18] H. Kisch, Semiconductor Photocatalysis: Principles and Applications, first ed., Wiley-VCH, Weinheim, 2015.
[19] V. Etacheri, C.D. Valentin, J. Schneider, D. Bahnemann, S.C. Pillai, Visible-light activation of TiO_2 photocatalysts: advances in theory and experiments, J. Photochem. Photobiol. C: Photochem. Rev. 25 (2015) 1–29.
[20] L.G. Devi, R. Kavitha, A review on non metal ion doped titania for the photocatalytic degradation of organic pollutants under UV/solar light: role of photogenerated charge carrier dynamics in enhancing the activity, Appl. Catal. B 140–141 (2013) 559–587.
[21] C. Ahn, J. Park, D. Kim, S. Jeon, Monolithic 3D titania with ultrathin nanoshell structures for enhanced photocatalytic activity and recyclability, Nanoscale 5 (2013) 10384–10389.
[22] C. Haw, W. Chiu, S.A. Rahman, P. Khiew, S. Radiman, R.A. Shukor, M.A.A. Hamid, N. Ghazali, The design of new magnetic-photocatalyst nanocomposites ($CoFe_2O_4$-TiO_2) as smart nanomaterials for recyclable-photocatalysis applications, New Journal of Chemistry, New J. Chem. 40 (2016) 1124–1136.
[23] D.H. Quiñones, A. Rey, P.M. Álvarez, F.J. Beltrán, P.K. Plucinski, Enhanced activity and reusability of TiO_2 loaded magnetic activated carbon for solar photocatalytic ozonation, Appl. Catal. B 144 (2014) 96–106.
[24] N. Kaur, S.K. Shahi, V. Singh, Synthesis, characterization and photocatalytic activity of magnetically separable γ-Fe_2O_3/N, Fe codoped TiO_2 heterojunction for degradation of Reactive Blue 4 dye, RSC Adv. 5 (2015) 61623–61630.
[25] S. Linley, T. Leshuk, F.X. Gu, Synthesis of magnetic rattle-type nanostructures for use in water treatment, ACS Appl. Mater. Interfaces 5 (2013) 2540–2548.
[26] B. Barrocas, O.C. Monteiro, M.E. Melo Jorge, S. Sério, Photocatalytic activity and reusability study of nanocrystalline TiO_2 films prepared by sputtering technique, Appl. Surf. Sci. 264 (2013) 111–116.
[27] K.P.O. Mahesh, D.-H. Kuo, B.-R. Huang, M. Ujihara, T. Imae, Chemically modified polyurethane-SiO_2/TiO_2 hybrid composite film and its reusability for photocatalytic degradation of Acid Black 1 (AB 1) under UV light, Appl. Catal. A 475 (2014) 235–241.
[28] D. Chen, R.A. Caruso, Recent progress in the synthesis of spherical titania nanostructures and their applications, Adv. Funct. Mater. 23 (2013) 1356–1374.
[29] J. Chen, Z. Hua, Y. Yan, A.A. Zakhidov, R.H. Baughmanm, L. Xu, Template synthesis of ordered arrays of mesoporous titania spheres, Chem. Commun. 46 (2010) 1872–1874.
[30] B. Liu, K. Nakata, M. Sakai, H. Saito, T. Ochiai, T. Murakami, K. Takagi, A. Fujishima, Hierarchical TiO_2 spherical nanostructures with tunable pore size, pore volume, and specific surface area: facile preparation and high-photocatalytic performance, Catal. Sci. Technol. 2 (2012) 1933–1939.
[31] P.T.N. Nguyen, C. Salim, W. Kurniawan, H. Hinode, A non-hydrolytic sol-gel synthesis of reduced graphene oxide/TiO_2 microsphere photocatalysts, Catal. Today 230 (2014) 166–173.
[32] J.H. Pan, Q. Wang, D.W. Bahnemann, Hydrous TiO_2 spheres: an excellent platform for the rational design of mesoporous anatase spheres for photoelectrochemical applications, Catal. Today 230 (2014) 197–204.
[33] B.F. Huang, D. Chen, X.Li. Zhang, R.A. Caruso, Y.-B. Cheng, Dual-Function scattering layer of submicrometer-sized mesoporous TiO_2 beads for high-efficiency dye-sensitized solar cells, Adv. Funct. Mater. 20 (2010) 1301–1305.
[34] K.-F. Du, D. Yang, Y. Sun, Controlled fabrication of porous titania beads by a sol-gel templating method, Ind. Eng. Chem. Res. 48 (2009) 755–762.
[35] H. Liu, Z. Bi, X.-G. Sun, R.R. Unocic, M.P.S. Paranthamanm Dai, G.M. Brown, Mesoporous TiO_2-B microspheres with superior rate performance for lithium ion batteries, Adv. Mater. 23 (2011) 3450–3454.
[36] L. Dou, L. Gao, X. Yang, X. Song, Hierarchical architectures TiO_2: Pollen-inducted synthesis remarkable crystalline-phase stability, tunable size, and reused photo-catalysis, J. Hazard. Mater. 203–204 (2012) 363–369.
[37] S. Ullah, E.P. Ferreira-Neto, A.A. Pasa, C.C.J. Alcântara, J.J.S. Acuña, S.A. Bilmes, M.L.M. Riccie, R. Landers, T.Z. Fermino, U.P. Rodrigues-Filho, Enhanced photocatalytic properties of core@shell SiO_2@TiO_2 nanoparticles, Appl. Catal. B 179 (2015) 333–343.
[38] D.G. Schukin, R.A. Caruso, Template synthesis and photocatalytic properties of porous metal oxide spheres formed by nanoparticle infiltration, Chem. Mater. 16 (2004) 2287–2292.
[39] T. Leshuk, S. Linley, G. Baxter, F. Gu, Mesoporous hollow sphere titanium dioxide photocatalysts through hydrothermal silica etching, ACS Appl. Mater. Interfaces 4 (2012) 6062–6070.
[40] D. Chen, L. Cao, F. Huang, P. Imperia, Y.-B. Cheng, R.A. Caruso, Synthesis of monodisperse mesoporous titania beads with controllable diameter high surface areas, and variable pore diameters (14–23 nm), J. Am. Chem. Soc. 132 (2010) 4438–4444.
[41] H.-J. Kim, J.-D. Jeon, S.-Y. Kwak, Highly dispersed mesoporous TiO_2 spheres via acid treatment and its application for dye-sensitized solar cells, Powder Technol. 243 (2013) 130–138.
[42] S. Tanaka, D. Nogami, N. Tsuda, Y. Miyake, Synthesis of highly-monodisperse spherical titania particles with diameters in the submicron range, J. Colloid Interface Sci. 334 (2009) 188–194.
[43] X. Jiang, T. Herricks, Y. Xia, Monodispersed spherical colloids of titania: synthesis, characterization, and crystallization, Adv. Mater. 15 (2003) 1205–1209.
[44] M. Pal, J.G. Serrano, P. Santiago, U. Pal, Size-controlled synthesis of spherical TiO_2 nanoparticles: morphology, crystallization, and phase transition, J. Phys. Chem. C 111 (2007) 96–102.
[45] E. Matijevíc, M. Budnik, L. Meites, Preparation and mechanism of formation of titanium dioxide hydrosols of narrow size distribution, J. Colloid Interface Sci. 61 (1977) 302–311.
[46] I.E. Saliby, L. Erdei, H.K. Shon, J.B. Kim, J.-H. Kim, Preparation and characterisation of mesoporous photoactive Na-titanate microspheres, Catal. Today 164 (2011) 370–376.
[47] L. Kong, C. Wang, H. Zheng, X. Zhang, Y. Liu, Defect-induced yellow color in Nb-doped TiO_2 and its impact on visible-light photocatalysis, J. Phys. Chem. C 119 (2015) 16623–16632.

[48] I. Krivtsov, M. Ilkaeva, V. Avdin, Z. Amghouz, S. Khainakov, J.R. García, E. Díaz, S. Ordóñez, Exceptional thermal stability of undoped anatase TiO_2 photocatalysts prepared by a solvent-exchange method, RSC Adv. 5 (2015) 36634–36641.
[49] Microtox® Manual, 1998.
[50] R. Morozov, I. Krivtsov, V. Avdin, Z. Amghouz, S.A. Khainakov, J.R. García, Peroxo method for preparation of composite silica-titania spheres, J. Non-cryst. Solids 435 (2016) 8–16.
[51] W. Stober, A. Fink, E. Bohn, Controlled growth of monodisperse silica spheres in the micron size range, J. Colloid Interface Sci. 26 (1968) 62–69.
[52] H.K. Singh, M. Saquib, M.M. Haque, M. Muneer, D.W. Bahnemann, Titanium dioxide mediated photocatalysed degradation of phenoxyacetic acid and 2,4,5-trichlorophenoxyacetic acid, in aqueous suspensions, J. Mol. Catal. A: Chem. 264 (2007) 66–72.
[53] https://www.epa.gov/sites/production/files/2015-06/documents/in_al_489_06241999.pdf (accessed 24 September 2016).
[54] H.-W. Chen, Y. Ku, Y.-L. Kuo, Effect of Pt/TiO_2 characteristics on temporal behavior of o-cresol decomposition by visible light-induced photocatalysis, Water. Res. 41 (2007) 2069–2078.
[55] K.-H. Wang, Y.-H. Hsieh, L.-J. Chen, The heterogeneous photocatalytic degradation, intermediates and mineralization for the aqueous solution of cresols and nitrophenols, J. Hazard. Mater. 59 (1998) 251–260.
[56] S. Rasalingam, H.S. Kibombo, C.-M. Wu, R. Peng, J. Baltrusaitis, R.T. Koodali, Competitive role of structural properties of titania-silica mixed oxides and a mechanistic study of the photocatalytic degradation of phenol, Appl. Catal. B 148–149 (2014) 394–405.
[57] M.F. Atitar, A.A. Ismail, S.A. Al-Sayari, D. Bahnemann, D. Afanasev, A.V. Emeline, Mesoporous TiO_2 nanocrystals as efficient photocatalysts: impact of calcination temperature and phase transformation on photocatalytic performance, Chem. Eng. J. 264 (2015) 417–424.
[58] Y. Lv, L. Yu, H. Huang, Y. Feng, D. Chen, X. Xie, Application of the soluble salt-assisted route to scalable synthesis of ZnO nanopowder with repeated photocatalytic activity, Nanotechnology 23 (2012) 065402.
[59] M. Antonopoulou, I. Konstantinou, Photocatalytic treatment of metribuzin herbicide over TiO_2 aqueous suspensions: removal efficiency, identification of transformation products, reaction pathways and ecotoxicity evaluation, J. Photochem. Photobiol. A: Chem. 294 (2014) 110–120.
[60] M. Antonopoulou, I. Konstantinou, Photocatalytic degradation and mineralization of tramadol pharmaceutical in aqueous TiO_2 suspensions: evaluation of kinetics, mechanisms and ecotoxicity, Appl. Catal. A: Gen. 515 (2016) 136–143.
[61] G.P.S. Marcone, Á.C. Oliveira, G. Almeida, G.A. Umbuzeiro, W.F. Jardim, Ecotoxicity of TiO_2 to Daphnia similis under irradiation, J. Hazard. Mater. 211–212 (2012) 436–442.
[62] V.K. Sharma, Aggregation and toxicity of titanium dioxide nanoparticles in aquatic environment—a review, J. Environ. Sci. Health A: Toxic Hazard. Subst. Environ. Eng. 44 (2009) 1485–1495.